

Surface Area of Early Visual Cortex Predicts Individual Speed of Traveling Waves During Binocular Rivalry

Erhan Genç^{1,2,3}, Johanna Bergmann^{1,3,4}, Wolf Singer^{1,3,5,6} and Axel Kohler^{1,3,7,8}

¹Department of Neurophysiology, Max Planck Institute for Brain Research, D-60528 Frankfurt am Main, Germany, ²Ruhr University Bochum, Biopsychology, D-44780 Bochum, Germany, ³Brain Imaging Center Frankfurt, D-60528 Frankfurt am Main, Germany, ⁴School of Psychology, University of New South Wales, Sydney, Australia, ⁵Ernst Strüngmann Institute (ESI) for Neuroscience in Cooperation with Max Planck Society, D-60528 Frankfurt am Main, Germany, ⁶Frankfurt Institute for Advanced Studies, Goethe University, D-60438 Frankfurt am Main, Germany, ⁷Institute of Psychology, University of Münster, D-48149 Münster, Germany and ⁸Current address: University of Osnabrück, Institute of Cognitive Science, Albrechtstr. 28, D-49076 Osnabrück, Germany

Address correspondence to Axel Kohler. Email: axel.kohler@uni-osnabrueck.de

Binocular rivalry ensues when different images are presented to the 2 eyes with conscious perception alternating between the possible interpretations. For large rivalry displays, perceptual transitions are initiated at one location and spread to other parts of the visual field, a phenomenon termed “traveling wave.” Previous studies investigated the underlying neural mechanisms of the traveling wave and surmised that primary visual cortex might play an important role. We used magnetic resonance imaging and behavioral measures in humans to explore how interindividual differences in observers’ subjective experience of the wave are related to anatomical characteristics of cortical regions. We measured wave speed in participants and confirmed the long-term stability of the individual values. Retinotopic mapping was employed to delineate borders of visual areas V1–V3 in order to determine surface area and cortical thickness in those regions. Only the surface areas of V1 and V2, but not V3 showed a correlation with wave speed. For individuals with larger V1/V2 area, the traveling wave needed longer to spread across the same distance in visual space. Our results highlight the role of early visual areas in mediating binocular rivalry and suggest possible mechanisms for the correlation between surface area and the traveling waves.

Keywords: binocular rivalry, interindividual differences, primary visual cortex, surface size, traveling wave

Introduction

Binocular rivalry has been described almost 2 centuries ago (Wheatstone 1838) as a process where disparate images presented separately to the 2 eyes compete for dominance in perception. Conscious experience alternates between these possible interpretations every few seconds. Often, perceptual switches are accompanied by a wave of change that starts at one location and spreads across the visual field (Meenes 1930; Pöppel et al. 1978). This so-called traveling wave of binocular rivalry has been studied using psychophysical (Wilson et al. 2001; Knapen et al. 2007; Paffen et al. 2008; Arnold et al. 2009; Kang et al. 2009, 2010; Naber et al. 2009; for a review see Kang and Blake 2011) and brain-imaging methods (Lee et al. 2005, 2007).

In the first dedicated investigation of the phenomenon, Wilson et al. (2001) specifically designed a circular binocular-rivalry stimulus (cf. Fig. 1) in order to measure the characteristics of the traveling wave with respect to known anatomical properties of visual cortex. They suggested, based on behavioral evidence only, that primary visual cortex (V1) might be the neural substrate of wave propagation. Using functional

magnetic resonance imaging (fMRI), Lee et al. (2005, 2007) found activity patterns in early visual areas V1–V3 corresponding to the propagation speed of traveling waves across the visual field, providing first direct evidence for the involvement of these cortical regions in transitions during binocular rivalry. Those results tied in nicely with the existing literature demonstrating a relationship between binocular-rivalry switches and activity changes in early visual areas even down to the lateral geniculate nucleus (Polonsky et al. 2000; Lee and Blake 2002; Haynes et al. 2005; Wunderlich et al. 2005). Also, transcranial magnetic stimulation over V1 has been shown to influence binocular-rivalry switches (Pearson et al. 2007). Nevertheless, the exact physiological mechanisms for the generation of traveling waves have not been elucidated yet.

One approach to find evidence for possible mechanisms is to investigate interindividual differences in perception and their underlying neuroanatomical correlates (for a review see Kanai and Rees 2011). For the processing of perceptual rivalry, 2 regions in parietal cortex have been identified that predict how long on average individuals settle for one perceptual interpretation before the next spontaneous switch in subjective experience occurs (Kanai et al. 2010, 2011). Transcranial magnetic stimulation in the same parietal regions influences alternation rates for different bistable paradigms (Carmel et al. 2010; Kanai et al. 2010, 2011; Zaretskaya et al. 2010), suggesting a general role of parietal cortex in the dynamics of perceptual switches.

In the current study, we investigated whether the anatomical characteristics of certain early visual regions would explain interindividual differences in the subjective experience of the traveling wave. We measured wave propagation times in a group of observers and also determined surface area and cortical thickness of visual areas V1, V2, and V3. For the behavioral as well as the anatomical measures, we conducted retests after 6 weeks (traveling wave) and 2 years (visual areas) in order to establish adequate reliability of the relevant variables before performing correlation analyses for the identification of the individual neural correlates underlying wave propagation during binocular rivalry.

Materials and Methods

Participants

Twenty-seven participants whose ages ranged from 18 to 34 (median, 23 years; 12 males) took part in the study. Twenty-three participants were right-handed and 4 left-handed as measured by the Edinburgh Handedness Inventory (Oldfield 1971), and none had any history of

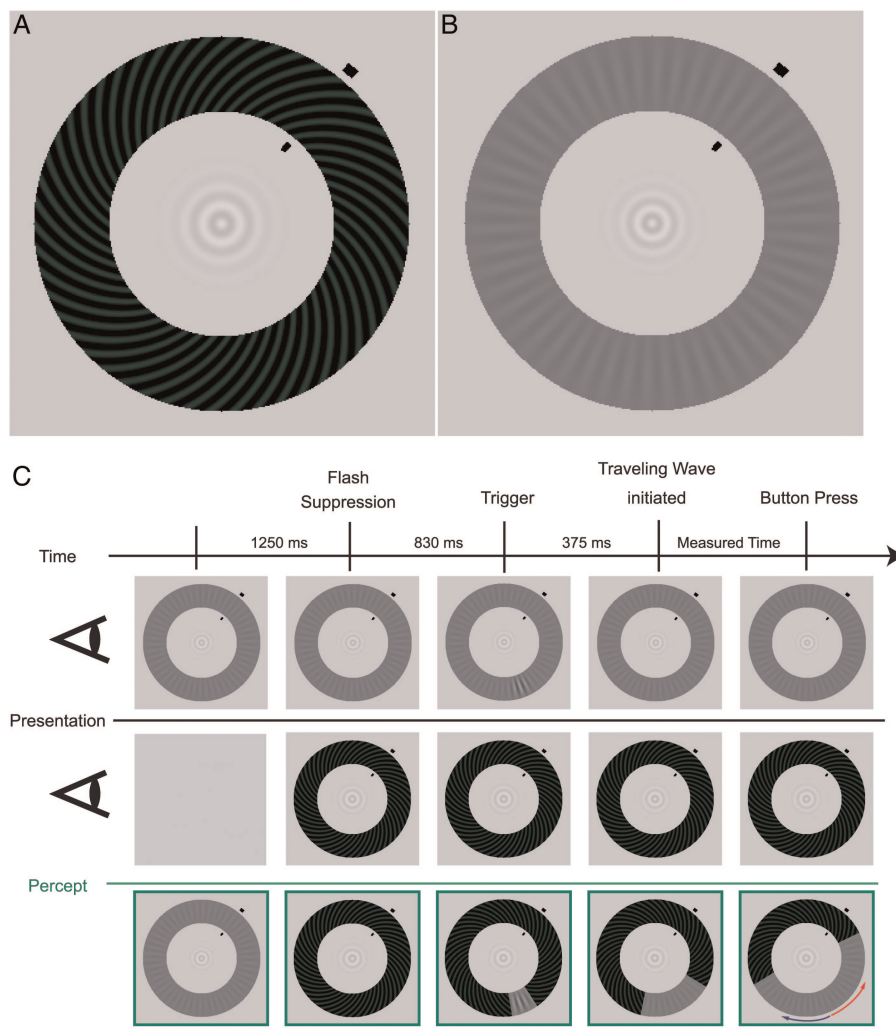


Figure 1. Stimuli and experimental procedure for the behavioral measurements (see Materials and Methods for a detailed description). (A) High-contrast spiral pattern (dominant stimulus). (B) Low-contrast radial pattern (target stimulus). Both stimuli are presented simultaneously to the separate eyes leading to a wave traveling along the annulus during perceptual switches. (C) While maintaining fixation on the small, central bull's-eye figure, participants monitored the perceptual wave that traveled along the shorter section between trigger location and arrival point (red arrow). The first 2 rows show the dissimilar images that are presented monocularly, while the green row at the bottom illustrates the resulting percept.

psychiatric or neurological disorders. All participants had normal or corrected-to-normal vision and were either paid for participation or received course credit. Written informed consent was obtained from all participants and the experimental procedures complied with the ethical regulations of the Max Planck Society and the relevant German legislation. Prior to the measurements, all aspects of the study were exposed to a mandatory Thesis Advisory Committee and carefully discussed. Participants were only included if they agreed with the procedures applied in case of incidental findings. These foresaw consultation with a neuroradiologist and information of the participant. For 18 participants, psychophysical tests took place in 2 sessions, with an interval of about 6 weeks between test and retest. We also acquired standard fMRI retinotopic-mapping scans from all participants and repeated the retinotopic-mapping scans for 14 participants after 2 years to compute the long-term stability of anatomical measures of the early visual areas.

Stimuli for Behavioral Experiment

We used 2 monocular, annularly shaped gratings similar to those described by Wilson et al. (2001) and Lee et al. (2005). The rivalry display consisted of a high-contrast spiral pattern of 50% Michelson contrast shown to one eye (see Fig. 1A), and a low-contrast radial-pattern display shown at 12% contrast to the other eye (see Fig. 1B). The high-contrast spiral pattern had a pitch angle of 45° and a spatial frequency

of 3.64 cycles/degree, with a faint greenish hue added to enhance the perceptual salience of the traveling wave (luminance: 7.7 cd/m^2 ; luminance of the dark phase: 2.54 cd/m^2). The spatial frequency of the grayish radial grating was 2.55 cycles/degree (luminance of the dark phase: 31.5 cd/m^2 ; luminance of the bright phase: 39.27 cd/m^2). The diameters of the outer edge of the 2 monocular annuli were 10 cm, corresponding to a visual angle of 7.85° . The annuli were 2 cm wide (1.6°). The inner edge had a diameter of 6 cm or 4.7° visual angle. In the center of the annuli was a bull's-eye-like fixation point. The spatial configuration of these narrow, annularly shaped rival targets effectively constrains the path of perceptual traveling waves, making it straightforward to induce the waves and measure their speed.

Stimuli and experimental procedure were generated in MATLAB 7.3.0 (R2006b) using Psychtoolbox 3.0.8 (Brainard 1997; Pelli 1997). Stimuli were presented on a 19" CRT monitor (1024×768 resolution, 120-Hz refresh rate). For the monocular projection of different images to the 2 eyes, participants wore Stereo Graphics Shutter Glasses that were synchronized with the monitor's refresh rate by a CrystalEyes Workstation (RealD, Beverly Hills, CA, USA).

Experimental Procedure

During the experiment, participants' head position was stabilized using a chin rest at a distance of 73 cm to the screen. Participants were

asked to maintain strict fixation on the bull's eye at the center of the annuli. We used the interocular flash-suppression technique introduced by Wolfe (1984). On each trial, the low-contrast radial pattern (the "target") was presented to one eye and then 1.25 s later the high-contrast spiral pattern was presented to the corresponding retinal location of the other eye. This sequence typically resulted in perceptual suppression of the target stimulus. After 0.83 s, an abrupt, local increment in the contrast of the radial target stimulus appeared for 0.375 s. The size of the increment was 3 spatial cycles (1.18°) of the radial grating, and it increased the contrast of the low-contrast grating locally from 12% to 27% (luminance of the dark phase: 23.0 cd/m², luminance of the bright phase: 40.1 cd/m²). As expected (Wilson et al. 2001), the abrupt onset of this increment triggered a change in perceptual dominance, causing the previously suppressed target pattern to become perceptually dominant immediately at the location of the trigger, which, in turn, tended to induce a wave of spreading dominance of the target that traveled around the annulus. Participants were instructed to press a button as soon as the wave reached an arrival point that was clearly designated by 2 short, black lines at the inner and outer boundaries of the annuli. Participants were asked to respond only to the wave that traveled along the shorter section between trigger and arrival point (see Fig. 1C). The background remained light gray (luminance: 91.8 cd/m²).

The trigger-point position varied between the different runs in relation to the arrival-point markers that were presented at 1 of 4 positions (40°, 140°, 220°, 320° in relation to the 12 o'clock position in the annuli) to cover all quadrants. The arrival-point markers and trigger-point position were always in different quadrants but in the same visual hemifields to ensure that waves induced by the triggers traveled along an intrahemispheric path. The distance between the arrival-point markers and the trigger point was 120° in rotation angle. The possible stimulus configurations were: arrival-point markers at 40° and trigger-point position 160° as seen in Figure 1C; arrival-point markers at 140° and trigger-point position at 20°; arrival-point markers at 220° and trigger-point position at 340°; arrival-point markers at 320° and trigger-point position at 220°. The time the wave needed to travel the distance of 7.38° in visual angle along the shorter path was measured based on the time elapsed from the appearance of the trigger to the participant's button press indicating that the wave had reached the arrival-point markers. After each trial, participants verified whether they had actually seen the trigger-induced wave traveling toward the arrival point and whether they had reacted in time by pressing a "yes" or "no" key. To control for participants' ocular dominance, the number of runs in which the target stimulus was presented to the right eye was equal to the number of runs in which it was presented to the left eye. Participants had to complete 8 runs consisting of at least 12 positive trials per trigger point, with negative trials (i.e., trials when waves were unsuccessfully triggered or when triggered waves dissipated before reaching the arrival-point markers) discarded from further analysis. In total, participants had to complete at least 96 trials in 1 session. Participants were familiarized with the instructions and the stimuli in 8 test trials, which preceded the actual experiment. For 18 participants, the same procedure was repeated after 6 weeks.

Analysis of Behavioral Data

Correlation and regression analyses were performed using R, version 2.10.1 (<http://www.R-project.org>) and the "car" package (<http://CRAN.R-project.org/package=car>). For all analyses, linear parametric methods were used, that is, Pearson coefficients for correlation and the general linear model for multiple regression. Statistical tests were performed using two-tailed tests with an α level of 0.05. Confidence intervals were estimated through a bootstrap technique with 1000 repetitions based on the R package "boot" (<http://CRAN.R-project.org/package=boot>). Data from the psychophysical measurements were corrected for outliers by removing trials with time estimates outside the range of 2 standard deviations from the mean for each individual.

Parametric correlation and regression analyses depend on a number of assumptions concerning the characteristics of the sample distributions (Cohen et al. 2003). We checked the parametric model assumptions with a global test (Peña and Slate 2006) available as a software package in R (<http://CRAN.R-project.org/package=gvlma>).

The test provides a global statistic combining the aspects linearity (form of the relationship), homoscedasticity (constant variance of residuals), uncorrelatedness, and normality. It also provides single statistics for each aspect if the global test indicates a violation of assumptions, so that the cause for model deviation can be identified.

Means were computed for intrahemispheric traveling-wave times (TWTs; wave start and end points in the same visual hemifield). The TWT estimates of 18 participants for the 2 test periods (separated by 6 weeks) were correlated to determine test-retest reliability of the behavior. Additionally, retinotopically defined anatomical measures of 14 participants for the 2 test periods (separated by 2 years) were correlated to determine the long-term stability of measures for the early visual areas.

For regression analyses of the relationship between TWT and anatomical measures of the visual areas, the average TWT of the 2 time points for the 18 retested participants and the TWT of the first time point for the remaining 9 participants was entered as dependent variable and the anatomical measures of visual field maps were entered as independent variables, either individually or in multiple-regression analyses. For the 14 participants with 2 scans, an average of the retinotopically defined anatomical measures for the 2 time points was computed and, for the remaining 4 participants, the retinotopically defined anatomical measures of the first session were entered as independent variables in the multiple-regression analyses.

Stimuli for Retinotopic Mapping

To obtain phase-encoded retinotopic preference maps of our participants we presented rotating wedge and expanding ring stimuli that create spatial sequences of neural activity in visual cortex (Engel et al. 1994; Sereno et al. 1995; Wandell et al. 2007). Stimuli were generated with a custom-made program based on the Microsoft DirectX library (Muckli et al. 2005) and presented using a MR-compatible goggle system (maximal visual field 24° vertical and 30° horizontal) with 2 organic light-emitting-diode displays (MR Vision 2000; Resonance Technology, Northridge, CA, USA). For the polar-angle mapping experiment, a wedge-shaped black and white checkerboard pattern was presented. The wedge spanned 22.5° of visual angle and extended to 15° from fixation. The wedge started at the right horizontal meridian and slowly rotated clockwise around the fixation point for a full circle of 360° (11.25° polar angle/volume [2000 ms]). The mapping experiment consisted of 12 repetitions of rotation, each cycle lasting for 64 s. For the eccentricity-mapping experiment, a ring-shaped checkerboard pattern flickering at a rate of 4 Hz was presented. The ring started with a radius of 1° and slowly expanded to a radius of 15° within 64 s. Seven cycles were repeated in the eccentricity run. Participants had no further task but to fixate on the central fixation point. The same procedure was repeated several months later for the retest.

Acquisition of Imaging Data

All data were acquired at the Brain Imaging Center Frankfurt am Main, Germany, using a Siemens 3-Tesla Trio scanner (Siemens, Erlangen, Germany) with a eight-channel head coil and maximum gradient strength of 40 mT/m.

Anatomical Imaging

For coregistration and anatomical localization of functional data, a T_1 -weighted high-resolution anatomical image of $1 \times 1 \times 1$ mm³ was acquired (MP-RAGE, TR = 2250 ms, TE = 2.6 ms, flip angle: 9°, FOV: 256 mm). The acquisition time for the anatomical image was 10 min, and the same measurement was repeated for the retest.

Retinotopic Mapping

For the polar-angle and eccentricity mapping experiment, a gradient-recalled echo-planar imaging (EPI) sequence with the following parameters was applied: 33 slices, TR = 2000 ms, TE = 30 ms, flip angle = 90°, FOV = 192 mm, slice thickness = 3 mm, gap thickness = 0.3 mm, voxel size = $3.0 \times 3.0 \times 3.0$ mm. The acquisition time for the whole retinotopic mapping was 22 min, and the same measurement was repeated for the retest.

Analysis of Imaging Data

We used FreeSurfer and FFAST (<http://surfer.nmr.mgh.harvard.edu>, version 5.1.0) to reconstruct cortical surfaces and perform functional data analysis.

Anatomical Data

The reconstruction of the cortical surface from the T_1 -weighted image was done using published surface-based methods in the FreeSurfer environment (<http://surfer.nmr.mgh.harvard.edu/fswiki/RecommendedReconstruction>); the details of the procedure have been described elsewhere (Dale et al. 1999; Fischl et al. 1999). The automatic reconstruction steps included Talairach transformation, skull stripping, white- (WM) and gray-matter (GM) segmentation, and reconstruction and inflation of the cortical surface. Inaccuracies for the automatic steps were corrected by manual editing, if necessary. To compute the long-term stability of the surface area and thickness for visual areas, the surface reconstruction procedure was done independently for the test and the retest sessions.

Functional Data

Preprocessing steps of all functional data was done using FFAST, including slice time correction, motion correction, and coregistration to the T_1 -weighted image, which was used to construct the cortical surface. For each participant, both functional runs from the test session were aligned to the T_1 -weighted image of the test and both functional runs from the retest session were aligned to the T_1 -weighted image of the retest. The time series of activation from each scan was examined using a Fourier transform. For each voxel, the amplitude and phase at stimulation frequency (here 12 cycles/run for the polar run and 7 cycles/run for the eccentricity run) was extracted. The phase angle of the response in a voxel at the stimulus rotation or dilation frequency is associated to the polar angle or eccentricity represented there. Finally, the phase angles were mapped to different pseudocolors whose intensity is an F -ratio between the squared amplitude of the response at the stimulus frequency with the average squared amplitudes at all other frequencies (excluding higher harmonics of the stimulus frequency and low-frequency signals). The resulting polar and eccentricity phase maps were displayed on the inflated cortical surface of the aligned T_1 -weighted image. The boundaries of the visual areas (V1, V2, and V3) were identified manually, for each participant and each session on the basis of phase-encoded retinotopy (Engel et al. 1994; Sereno et al. 1995) and subsequent calculation of the visual field signs (Sereno et al. 1995; Dumoulin et al. 2003; Schwarzkopf et al. 2011). In addition to the first rater, who was the first author, a second rater, an intern in our laboratory who was completely unaware of the behavioral results or the aim of the study also delineated the visual areas based on the visual field signs to exclude any potential bias for the correlations between behavioral and anatomical data we observed. Delineation of the visual

areas based on the visual field signs enhances the objectivity of the procedure and can also be done without prior anatomical knowledge of the visual areas (Sereno et al. 1995; Pitzalis et al. 2006). The delineations of both raters were averaged for the 2 time points and were then correlated with each other to compute the inter-rater reliability. In addition to the functional delineation of the visual areas, we also defined the surface area of the entire V1 by a probabilistic method implemented in FreeSurfer; the details of the procedure have been described elsewhere (Hinds et al. 2008; Schwarzkopf and Rees 2013). We used a conservative probability threshold of 0.8 to define the vertices on the cortical surface representing the anatomical V1 (note that very similar results were observed for other lower [0.7] or higher [0.9] probabilistic thresholds). Finally, the surface area and the average cortical thickness for each region were determined by FreeSurfer's algorithm for surface and cortical thickness calculation.

Voxel-Based Morphometry

In addition to the region-of-interest-based approach we also conducted a whole-brain voxel-based morphometry (VBM) analysis of GM density (Ashburner and Friston 2000) on the same set of T_1 -weighted MR images from the first session. By using the segmentation tools in SPM8 (<http://www.fil.ion.ucl.ac.uk/spm/>), we first segmented the T_1 -weighted MR images for GM and WM. Next, we performed diffeomorphic anatomical registration through exponentiated lie algebra (Ashburner 2007) for intersubject registration of the GM images. The registered GM images were smoothed with a Gaussian kernel (FWHM = 8 mm) and then transformed to Montreal Neurological Institute stereotaxic space for multiple-regression analysis. Age and sex were included in the design matrix as covariates of no interest. For the whole-brain analyses, we used a family-wise-error-corrected P value of 0.05 to detect voxels that were significantly correlated with the individual TWTs. We also computed VBM analyses based on small-volume-corrected (SVC) statistics. We used V1, V2, and V3 as a combination or separately as prior regions of interest (ROIs) for the SVC analyses. The ROIs were defined probabilistically by using the SPM Anatomy Toolbox (Eickhoff et al. 2005).

Results

Although the stimulus configuration (Fig. 1) was identical for all observers, we found a large interindividual variability for the TWT ($M = 1876$ ms, $SD = 817$ ms), but a high test-retest reliability in the group of 18 participants over 6 weeks ($r_{16} = 0.79$, $P < 0.001$; Fig. 2A,B). No significant sex differences were found for the average TWT ($t_{25} = 0.52$, $P = 0.68$). We also acquired standard fMRI retinotopic-mapping scans from all participants and repeated

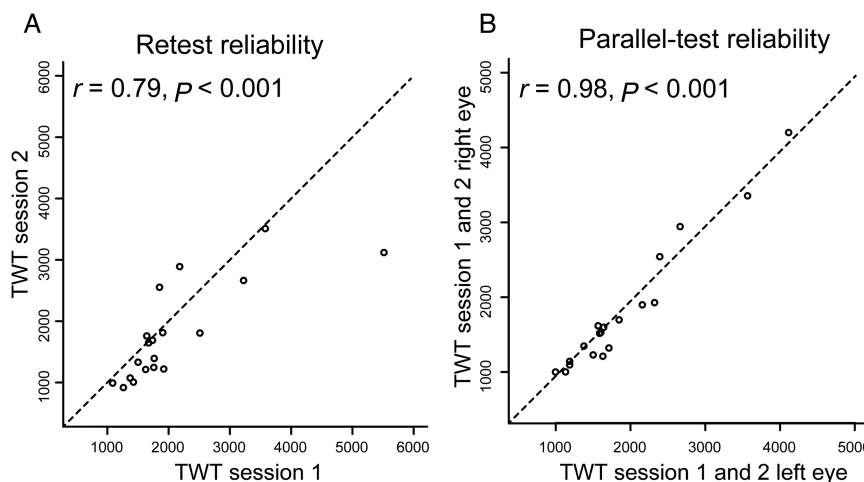


Figure 2. Reliabilities of the behavioral measure for the group of 18 participants. (A) The analysis shows high test-retest reliability for TWT after 6 weeks. (B) The analysis also shows high parallel-test reliability for TWT demonstrating that this psychophysical measure is a stable feature in individual participants.

Table 1

Age, gender, intrahemispheric traveling wave times (TWT), surface area and cortical thickness for retinotopic areas V1–V3, whole-brain surface and volume for all individual participants

Participants			Behavioral measure	Anatomical measures							
Participant	Age	Gender	TWT (ms)	Surface area (mm ²)			Cortical thickness (mm)			Whole-brain surface in (mm ²)	Whole-brain volume (mm ³)
				V1	V2	V3	V1	V2	V3		
BKM30	34	Male	1546	4144	3487	2368	1.96	2.07	2.29	190 128	538 828
CGA21	23	Male	1591	4246	3059	2360	1.91	2.21	2.34	187 747	563 187
CRD21	22	Female	1365	3322	3241	2633	1.76	1.91	2.22	178 921	528 874
CSN03	25	Male	1620	3805	4169	3328	1.84	2.03	2.24	202 237	574 201
FDN14	27	Male	999	3682	3010	3192	1.89	2.07	2.30	203 109	575 618
GPS10	25	Male	1787	4504	3617	2907	1.95	2.00	2.28	204 087	571 383
KHA29	22	Female	1152	2938	2722	2258	1.74	1.98	2.22	159 871	464 136
KKA06	23	Female	2138	4230	3861	2906	1.70	1.85	2.21	185 511	499 928
LAA30	26	Female	3463	5367	3971	3340	1.83	2.25	2.31	183 378	527 725
MHD11	21	Male	2815	5127	3898	3401	1.83	2.20	2.31	164 147	493 029
MOA30	22	Female	1166	4518	3380	2769	2.02	2.29	2.40	164 311	483 185
NMR26	27	Male	1549	4140	3516	3212	1.84	2.15	2.42	180 674	545 645
RAA22	22	Female	2465	4364	3275	2629	1.59	1.95	2.39	189 213	570 974
RCR06	24	Female	1062	4201	3580	2625	1.74	1.95	1.99	172 605	454 357
RKL25	27	Male	4162	6296	4585	2716	1.99	2.14	2.44	189 815	550 345
SDA01	21	Male	1572	3612	3301	2916	1.56	1.99	2.16	194 343	570 296
STA17	28	Female	2014	4091	3347	2089	1.75	2.20	2.39	174 250	495 167
TGA01	21	Female	1361	4828	3460	2929	1.72	2.03	2.08	191 794	559 935
BRA09	26	Female	1642	4621	3884	2893	1.89	2.10	2.44	196 342	574 720
UHS29	23	Male	1270	4566	3734	3439	1.81	2.15	2.32	208 922	573 270
USA13	26	Female	2669	4404	4470	3023	1.91	2.38	2.62	182 327	547 862
GPS03	21	Male	1278	4148	3341	2998	1.75	1.98	2.30	207 721	629 895
CBA19	20	Female	3261	4280	3621	1968	1.85	2.01	2.24	178 806	500 319
CSA11	18	Female	1528	3427	2735	2118	1.85	2.35	2.55	186 730	587 153
CSI02	18	Female	1097	3135	2925	1812	1.78	2.14	2.28	150 770	434 979
EMP05	21	Male	1439	4107	3498	2537	1.73	2.10	2.14	202 843	556 551
KVA20	24	Female	2662	3730	4129	2924	1.74	2.01	2.08	175 026	470 832

the retinotopic mapping for a subgroup ($N=14$) after 2 years to compute the long-term stability for the anatomical measures (surface area, cortical thickness; Table 1) of the early visual areas (V1, V2, and V3; Fig. 3 and Supplementary Fig. 1). For all 3 areas, we found high long-term test–retest reliabilities (V1 surface area, $r_{(12)}=0.87$, $P<0.001$, V1 cortical thickness, $r_{(12)}=0.83$, $P<0.001$; V2 surface area, $r_{(12)}=0.86$, $P<0.001$, V2 cortical thickness, $r_{(12)}=0.81$, $P<0.001$; V3 surface area, $r_{(12)}=0.86$, $P<0.001$; V3 cortical thickness, $r_{(12)}=0.70$, $P=0.005$). Correlations between surface areas of the different regions showed that V1 and V2 are strongly correlated ($r_{(25)}=0.67$, $P<0.001$), with an intermediate value for V2 and V3 ($r_{(25)}=0.53$, $P=0.005$), and the weakest coefficient for V1 and V3 ($r_{(25)}=0.41$, $P<0.04$), a trend already observed in a previous study by Dougherty et al. (2003). We found hemispheric differences (right > left) in surface area for V2 ($t_{26}=-3.29$, $P=0.003$) and V3 ($t_{26}=-2.66$, $P=0.013$) but not for V1 ($t_{26}=-0.94$, $P=0.35$). On the behavioral level, there were no significant differences between TWT values in the right and left hemifields ($t_{26}=0.09$, $P=0.93$) and the correlation between the 2 measures was at ceiling level ($r_{(25)}=0.95$, $P<0.001$). For these reasons, we collapsed data across hemispheres and hemifields.

In addition to the area boundaries defined by an experienced rater (first author), we also used boundaries determined by a naïve rater on the basis of field-sign maps (see Materials and Methods). The agreement between raters was high (V1 surface area, $r_{(12)}=0.95$, $P<0.001$, V1 cortical thickness, $r_{(12)}=0.99$, $P<0.001$; V2 surface area, $r_{(12)}=0.82$, $P<0.001$, V2 cortical thickness, $r_{(12)}=0.97$, $P<0.001$; V3 surface area, $r_{(12)}=0.64$, $P=0.013$; V3 cortical thickness, $r_{(12)}=0.80$, $P=0.001$). Since the pattern of results was virtually identical for the 2 raters, the average of the test and retest values of the experienced rater was used for all further analyses.

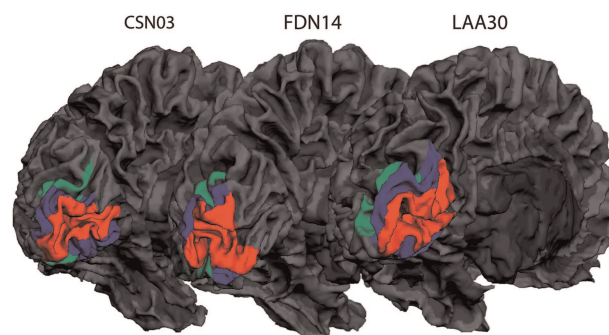


Figure 3. Variability in cortical surface size of early visual areas. Representative maps of 3 participants showing cortical regions V1–V3 on a reconstructed 3D mesh of the left hemisphere. Red indicates V1, blue indicates V2, and green indicates V3.

For all correlations and regressions, a global test of the assumptions for parametric approaches (general linear model) was performed before proceeding with the analysis (Peña and Slate 2006; see Materials and Methods). All assumptions were met ($P>0.05$) except for skewness in V3 ($P=0.008$), indicating an asymmetric distribution of the regression residuals. Correlations between surface area and cortical thickness of visual areas V1–V3 and the behavioral TWT measure were computed. Separate bivariate analyses for the visual areas showed that the surface areas of V1 ($r_{(25)}=0.67$, $P<0.001$, 95% CI 0.24, 0.85) and V2 ($r_{(25)}=0.67$, $P=0.001$, 95% CI 0.42, 0.83) were significantly correlated with TWT (Fig. 4). No significant correlation was found between TWT and the surface area of V3 ($r_{(25)}=0.10$, $P=0.62$, 95% CI -0.32 , 0.49). In a direct comparison between the coefficients, the correlations for V1 ($t=3.48$, $P=0.002$) and V2 ($t=4.14$, $P<0.001$) were significantly larger than the V3 value. Using surface sizes normalized to the

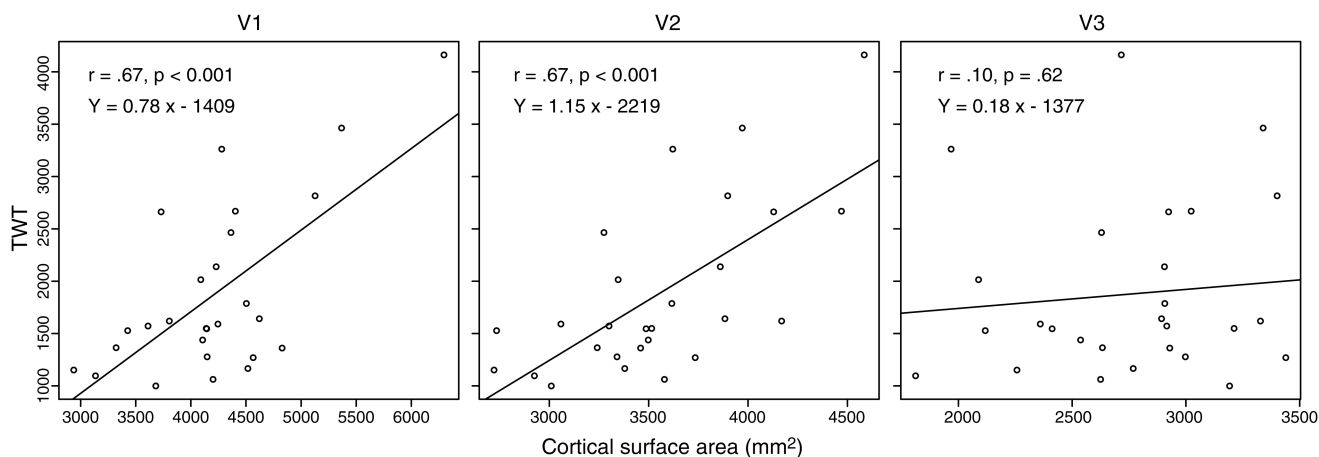


Figure 4. Correlation between behavioral measure and cortical surface of visual areas. Bivariate correlation analyses showed that cortical surface area of V1 and V2 predict behavioral variance in TWT; no relationship was found between TWT and cortical surface area of V3.

overall cortical surface area (V1/V2/V3 area divided by the surface area of both hemispheres), resulted in smaller effect sizes with the same general trend (V1: $r_{(25)} = 0.63, P < 0.001$; V2: $r_{(25)} = 0.62, P = 0.001$; V3: $r_{(25)} = 0.10, P = 0.62$). In contrast to surface area, we found that cortical thickness of the visual areas was not associated with TWT (V1: $r_{(25)} = 0.15, P = 0.44$; V2: $r_{(25)} = 0.17, P = 0.39$; V3: $r_{(25)} = 0.24, P = 0.23$).

In a combined multiple-regression analysis with surface areas from the early visual regions as independent variables and TWT as dependent variable, surface areas of V1, V2, and V3 all provided unique contributions to TWT prediction (V1: $\beta = 0.43, t_{23} = 2.52, P = 0.02$; V2: $\beta = 0.58, t_{23} = 3.13, P = 0.01$; V3: $\beta = -0.38, t_{23} = -2.55, P = 0.02$). Note that only V3 has a negative β coefficient and did not show a significant bivariate correlation with TWT ($r = 0.10$, see above). This condition, in which an independent variable shows no bivariate correlation with the dependent variable, but makes a significant contribution in the context of a multiple-regression analysis with other variables, is called “suppression” in statistics. The variable suppresses variance that is not related to the dependent measure in other independent variables and thereby enhances predictive power of the variable set as a whole (Cohen et al. 2003). Only the surface areas of V1 and V2 are directly associated with TWT, showing partly independent contributions indicated by the significant beta coefficients. Consequently, the variance in TWT explained by the combination of all 3 surface areas amounts to a large effect size of about 60% ($R^2 = 0.63, 95\% \text{ CI } 0.35, 0.84$; adjusted $R^2 = 0.59, 95\% \text{ CI } 0.28, 0.82$).

Correlations might be due to common influence from third variables. Therefore, we controlled for the effects of age, sex, whole-brain surface area, and whole-brain volume on the regression analyses. To rule out the influence from third variables, we computed a multiple-regression analysis with surface areas of V1, V2, V3, age, sex, whole-brain surface area, and whole-brain volume as independent variables and TWT as dependent variable. The strong and unique relationship between the surface areas of V1/V2 and TWT remained stable (V1: $\beta = 0.44, t_{(19)} = 2.34, P = 0.03$; V2: $\beta = 0.60, t_{(19)} = 2.78, P = 0.01$; other predictors, $P > 0.08$). Separate correlation analyses for the 4 control variables did not reveal any significant associations with TWT (age: $r_{(25)} = 0.16, P = 0.42$; sex: $r_{(25)} = -0.08, P$

$= 0.68$; whole-brain surface area: $r_{(25)} = 0.02, P = 0.92$; whole-brain volume: $r_{(25)} = -0.06, P = 0.75$).

As an alternative to the functional definition of primary visual cortex, Hinds et al. (2008, 2009) could demonstrate that the location of cortical folds at the occipital pole provide a good anatomical estimate of the location of V1 and its areal extent. We applied their probabilistic map at a threshold of 0.8 as implemented in the FreeSurfer software (other thresholds provided almost identical results). First, the correlation between our functional V1 size and the Hinds estimate was only moderate, $r_{(25)} = 0.41, P = 0.04$, suggesting a shared variance of $<20\%$ ($r^2 = 0.17$). Second, the correlation with TWT was not significant ($r_{(25)} = 0.12, P = 0.57$). This finding is in agreement with a study by Schwarzkopf and Rees (2013), where they found exactly the same pattern of results in their dataset: The correlation between anatomical and functional estimate was of similar, moderate magnitude ($r = 0.37$) and the correlation to a behavioral measure of a visual illusion was not significant ($r = 0.11$) in contrast to the correlation using the functional surface estimate from retinotopic mapping. This implies that mainly the variance associated with the representation of the central part of the visual field is predictive of interindividual differences in the subjective experience of visual illusions and not necessarily the overall anatomical extent of V1.

In addition to the analyses focusing on early visual areas, we used whole-brain VBM to investigate whether anatomical features of other regions also correlate with TWT. VBM is based on the segmentation of GM and WM and identifies voxels in which the density of GM is correlated with the relevant behavioral measure. We did not find any significant cluster at a level of $P < 0.05$ (whole brain, FWE-corrected). Also, small-volume corrections for the areas V1–V3 separately or combined did not produce any significant results (FWE-corrected). However, this negative finding might be due to the small sample size ($N = 27$), which limits the statistical power of the whole-brain analysis.

Discussion

Our results showed that the propagation time of traveling waves is positively correlated with the surface area of early visual areas V1 and V2, but not V3. A multiple-regression

analysis demonstrated that the contributions of all early visual areas combined explained about 60% of the variance in wave speed, underlining the role of early visual processing stages in mediating binocular rivalry.

Already in the original publication on the traveling wave (Wilson et al. 2001), it was surmised that properties of V1 might explain the characteristic spread of perceptual transitions. Later fMRI studies found that activity in all 3 areas V1–V3 were associated with perceptual switches (Lee et al. 2005). In a follow-up study by the same authors (Lee et al. 2007), only V1, but not V2 and V3, showed wave-related activity under conditions when attention was diverted away from the stimulus and observers were presumably unaware of the perceptual changes, although those activity changes might have been induced by other mechanisms (Moradi and Heeger 2009), since binocular rivalry seems to be abolished during periods of inattention (Zhang et al. 2011; Brascamp and Blake 2012). Our data confirm the association between early visual cortex and binocular rivalry and, in addition, demonstrate that V1/V2 anatomy explains the differences between individual observers, with larger V1/V2 sizes predicting longer wave durations. Note, however, that our correlative approach cannot differentiate whether wave propagation is mediated by local horizontal connections or feedback from higher visual areas.

For the visual system, the first study relating individual capacities of observers to properties of visual cortex showed that visual acuity was related to the retinotopic organization of V1 (Duncan and Boynton 2003). Schwarzkopf et al. (2011), Schwarzkopf and Rees (2013) found that the size of V1 was related to the individual strength of 2 well-known visual size illusions. In our own previous experiments, we described how the quality of connections through the corpus callosum between different visual areas determines the perception of a bistable motion stimulus (Genç et al. 2011a) and the propagation of traveling waves across the brain hemispheres (Genç et al. 2011b).

Anatomical studies show correlated size variations among processing structures in the human visual system. There is a strong association of V1 surface area and volume with the size of the lateral geniculate nucleus and a weaker correlation with the cross-sectional area of the optic tract (Andrews et al. 1997). Genetic and twin studies suggest that there is a common developmental factor determining this size covariation in the visual system (Chen et al. 2011, 2012; Bakken et al. 2012). Dougherty et al. (2003) found that V1 and V2 surface areas are strongly correlated, whereas V1 and V3 are not. The breakdown of size covariation for V3 agrees with the present finding that correlations between traveling-wave speed and surface area were only significant for V1 and V2, but not V3. The specificity of this association was not due to differences in reliabilities of the surface measures in the visual areas, since the long-term stability for the measures in V1, V2, and V3 were of similar magnitude ($r \approx 0.80$) in the data from the experienced rater. Note however that there was a drop-off in inter-rater agreement in V3 compared with V1 and V2. This might still reflect differences in the quality of anatomical measures for the different visual areas, which should be considered in future work.

In previous studies, Schwarzkopf et al. (2011), Schwarzkopf and Rees (2013) found that the strengths of 2 visual illusions (Ebbinghaus and Ponzo illusion) were negatively correlated with V1 but not V2 and V3 size. They interpreted their findings in accordance with presumed effects of size scaling on the

organization of local neural networks. With increasing size of an area, it is thought that single neural elements and their processes do not scale proportionately to area size (Kaas 2000) and therefore cover a smaller part of the sensory space, that is, the visual field in this case (Kanai and Rees 2011). In human anatomical studies, it has indeed been found that V1 and V2 surface areas correlate positively with the number of neurons in these regions (Leuba and Garey 1987). This suggests that the cortical extent of lateral interactions does not increase with increasing surface area. This has 2 consequences. First, for a given spacing of contours in visual field coordinates, interactions between these contours should be weaker in larger cortices because their cortical representations would be more widely spaced. This could account for the reduced strength of the illusions in the Schwarzkopf et al. studies (Kanai and Rees 2011). Second, propagation speed of lateral interactions—in the present case, the traveling wave—would be consistent across the cortical tissue but correspond to slower movements in visual field coordinates as cortical surface increases. This might account for the positive correlation between wave duration and V1 size in our study.

However, we only used the whole retinotopically mapped surface area for correlation analyses. Ideally, one would have considered only the segments of V1–V3 representing the trajectory of the traveling-wave. In our case, the cortical representations of the traveling wave in V1–V3 were near the foveal confluence, where unequivocal separation of areas is difficult and requires advanced techniques (cf., Schira et al. 2009). Since we lacked such explicit mappings, we decided to rely on surface estimates of the whole areas. But there are other variables that correlate with overall V1 surface area and might explain its predictive value for traveling-wave speed. It has been demonstrated with magnetic resonance spectroscopy and magnetoencephalography that the concentration of the inhibitory neurotransmitter γ -aminobutyric acid (GABA) in human V1 is positively correlated with performance in an orientation-discrimination task and the frequency of visually induced gamma oscillations (Edden et al. 2009; Muthukumaraswamy et al. 2009). Gamma-oscillation frequency, in turn, has a strong genetic component (van Pelt et al. 2012) and increases with the surface area of V1 and V2 (Schwarzkopf et al. 2012). Therefore, it is possible that larger V1 size is also associated with higher GABA concentration. Inhibitory interactions between competing neural populations are a central part in computational models of binocular rivalry (Wilson et al. 2001; Kang et al. 2010) and direct relations exist also between binocular rivalry and the modulation of gamma oscillations in V1 (Fries et al. 1997, 2001). In addition, the network of GABA-ergic interneurons has important pacemaker functions in the generation of gamma oscillations (for a review see Uhlhaas et al. 2009). Interindividual variations in GABA-ergic mechanisms and/or frequency of gamma oscillations might therefore be relevant factors for a mechanistic explanation of the effect of V1 size on wave speed.

In addition to the dissociation between V1/V2 and V3 surfaces, respectively, we were also able to demonstrate a dissociation between surface area and cortical thickness: Although both anatomical measures showed high long-term and inter-rater reliabilities, only surface size is a significant predictor of traveling waves. As might be expected, this suggests that only the lateral, but not the vertical organization of V1/V2 has an influence on the perceived spread of activity in the cortical sheet. The development of the neocortex is characterized

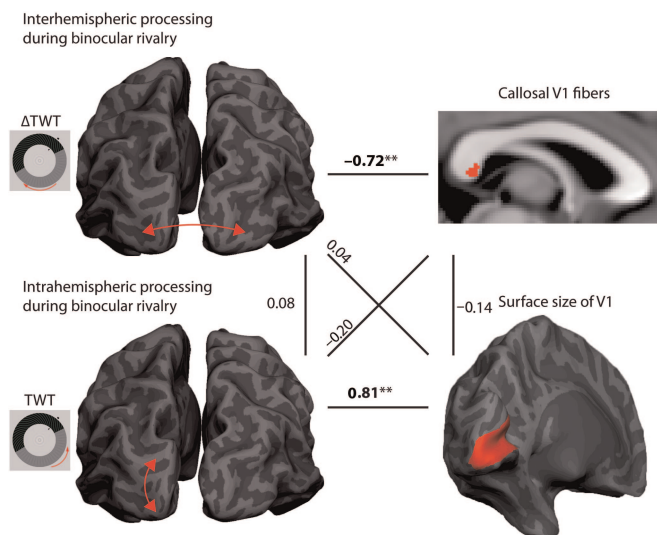


Figure 5. Relationships between inter- and intrahemispheric interactions during binocular rivalry. The figure provides an overview of the main findings in connection with the results of a previous study (Genç et al. 2011b). The interhemispheric delay of traveling binocular-rivalry waves (Δ TWT = interhemispheric TWT – intrahemispheric TWT) shows a specific relationship to properties of callosal fibers that connect the primary visual cortices of the 2 hemispheres (see horizontal line on top). In addition, intrahemispheric processing of these waves is strongly related to the surface size of V1 (see horizontal line on bottom). Interestingly, these structure–function relationships are highly specific and show much weaker and nonsignificant associations with each other in cross-correlation analyses (see diagonal lines). Therefore, the 2 behavioral features are stable within an individual, but independent of each other. This dissociation is probably due to the lack of dependence on the structural level (see vertical lines).

by 2 distinct stages: an early phase of symmetrical cell division and a later phase of asymmetrical division. The former presumably determines surface area of a cortical region and the latter cortical thickness (Kornack and Rakic 1995; Rakic 1995). This hypothesis is compatible with large-scale anatomical studies in humans showing that cortical thickness and surface area are controlled by independent genetic factors (Panizzon et al. 2009; Winkler et al. 2010). From a methodological perspective, correlations with cortical thickness measures might have been concealed due to limited interindividual variation, although test–retest reliabilities were high ($r > 0.70$).

In a previous study on the traveling wave, we used diffusion tensor imaging (DTI) to investigate the relationship between visual-cortex fiber connections through the corpus callosum and interhemispheric propagation of the traveling wave (Genç et al. 2011b). When the traveling wave has to cross between the left and right visual hemifields, there is a slight delay in the propagation time presumably due to the transfer of information between brain hemispheres (Wilson et al. 2001). DTI measures of callosal microstructure were associated with individual delay values only for V1 segments in the corpus callosum with a trend for V2, in accordance with our current results on individual propagation times within hemispheres. A comparison between propagation times and interhemispheric delay in the same group of 18 participants demonstrates a double dissociation of the behavioral measures with the respective intrahemispheric (surface area) and interhemispheric (corpus-callosum microstructure) components (Fig. 5) and no covariation of the structural parameters. This suggests independent developmental trajectories and genetic determinants of visual-cortex organization for surface area and interhemispheric connectivity.

In summary, interindividual variation in the subjective experience of the traveling wave shows a strong association with the surface size of early visual areas V1 and V2. This effect is independent of other anatomical features of those regions like cortical thickness and interhemispheric connectivity. Further experiments are needed to investigate the exact physiological mechanisms mediating the influence of cortical surface area on the propagation of traveling waves.

Supplementary Material

Supplementary Material can be found at <http://www.cercor.oxfordjournals.org/> online.

Funding

This work was supported by the Max Planck Society and the Federal Ministry of Education and Research in Germany (BMBF 01 GO 0508).

Notes

The authors thank Arjen Alink, Luiz Lana, Kerstin Schmidt, Caspar Schwiedrzik, Sarah Weigelt, Michael Wübral, and Ulf Ziemann for helpful discussions on design and interpretation of the experiments as well as Ralf Deichmann, Sandra Anti, Steffen Volz, Ulrike Nöth, and Thomas Sattler for support with the MRI measurements. The authors especially thank Nadine Brehm for delineating the visual areas as the second rater. They also thank Randolph Blake and Frank Tong for discussions on the interpretation of the results and for comments on the manuscript. The authors declare no competing financial interests. *Conflict of Interest:* None declared.

References

- Andrews TJ, Halpern SD, Purves D. 1997. Correlated size variations in human visual cortex, lateral geniculate nucleus, and optic tract. *J Neurosci.* 17:2859–2868.
- Arnold DH, James B, Roseboom W. 2009. Binocular rivalry: spreading dominance through complex images. *J Vis.* 9:4.
- Ashburner J. 2007. A fast diffeomorphic image registration algorithm. *Neuroimage.* 38:95–113.
- Ashburner J, Friston KJ. 2000. Voxel-based morphometry—the methods. *Neuroimage.* 11:805–821.
- Bakken TE, Roddey JC, Djurovic S, Akshoomoff N, Amaral DG, Bloss CS, Casey BJ, Chang L, Ernst TM, Gruen JR et al. 2012. Association of common genetic variants in GPCPD1 with scaling of visual cortical surface area in humans. *Proc Natl Acad Sci USA.* 109:3985–3990.
- Brainard DH. 1997. The psychophysics toolbox. *Spat Vis.* 10:433–436.
- Brascamp JW, Blake R. 2012. Inattention abolishes binocular rivalry: perceptual evidence. *Psychol Sci.* 23:1159–1167.
- Carmel D, Walsh V, Lavie N, Rees G. 2010. Right parietal TMS shortens dominance durations in binocular rivalry. *Curr Biol.* 20:R799–R800.
- Chen CH, Gutierrez ED, Thompson W, Panizzon MS, Jernigan TL, Eyer LT, Fennema-Notestine C, Jak AJ, Neale MC, Franz CE et al. 2012. Hierarchical genetic organization of human cortical surface area. *Science.* 335:1634–1636.
- Chen CH, Panizzon MS, Eyer LT, Jernigan TL, Thompson W, Fennema-Notestine C, Jak AJ, Neale MC, Franz CE, Hamza S et al. 2011. Genetic influences on cortical regionalization in the human brain. *Neuron.* 72:537–544.
- Cohen J, Cohen P, West SG, Aiken LS. 2003. Applied multiple regression/correlation analysis for the behavioral sciences. Mahwah, NJ: Lawrence Erlbaum.

- Dale AM, Fischl B, Sereno MI. 1999. Cortical surface-based analysis. I. Segmentation and surface reconstruction. *Neuroimage*. 9:179–194.
- Dougherty RF, Koch VM, Brewer AA, Fischer B, Modersitzki J, Wandell BA. 2003. Visual field representations and locations of visual areas V1/2/3 in human visual cortex. *J Vis*. 3:586–598.
- Dumoulin SO, Hoge RD, Baker CL Jr, Hess RF, Achtman RL, Evans AC. 2003. Automatic volumetric segmentation of human visual retinotopic cortex. *Neuroimage*. 18:576–587.
- Duncan RO, Boynton GM. 2003. Cortical magnification within human primary visual cortex correlates with acuity thresholds. *Neuron*. 38:659–671.
- Edden RAE, Muthukumaraswamy SD, Freeman TCA, Singh KD. 2009. Orientation discrimination performance is predicted by GABA concentration and gamma oscillation frequency in human primary visual cortex. *J Neurosci*. 29:15721–15726.
- Eickhoff S, Stephan KE, Mohlberg H, Grefkes C, Fink GR, Amunts K, Zilles K. 2005. A new SPM toolbox for combining probabilistic cytoarchitectonic maps and functional imaging data. *NeuroImage*. 25:1325–1335.
- Engel SA, Rumelhart DE, Wandell BA, Lee AT, Glover GH, Chichilnisky EJ, Shadlen MN. 1994. fMRI of human visual cortex. *Nature*. 369:525.
- Fischl B, Sereno MI, Dale AM. 1999. Cortical surface-based analysis. II: inflation, flattening, and a surface-based coordinate system. *Neuroimage*. 9:195–207.
- Fries P, Roelfsema PR, Engel AK, König P, Singer W. 1997. Synchronization of oscillatory responses in visual cortex correlates with perception in interocular rivalry. *Proc Natl Acad Sci USA*. 94:12699–12704.
- Fries P, Schröder JH, Singer W, Engel AK. 2001. Conditions of perceptual selection and suppression during interocular rivalry in strabismic and normal cats. *Vision Res*. 41:771–783.
- Genç E, Bergmann J, Singer W, Kohler A. 2011a. Interhemispheric connections shape subjective experience of bistable motion. *Curr Biol*. 21:1494–1499.
- Genç E, Bergmann J, Tong F, Blake R, Singer W, Kohler A. 2011b. Callosal connections of primary visual cortex predict the spatial spreading of binocular rivalry across the visual hemifields. *Front Hum Neurosci*. 5:161.
- Haynes JD, Deichmann R, Rees G. 2005. Eye-specific effects of binocular rivalry in the human lateral geniculate nucleus. *Nature*. 438:496–499.
- Hinds O, Polimeni JR, Rajendran N, Balasubramanian M, Amunts K, Zilles K, Schwartz EL, Fischl B, Triantafyllou C. 2009. Locating the functional and anatomical boundaries of human primary visual cortex. *Neuroimage*. 46:915–922.
- Hinds OP, Rajendran N, Polimeni JR, Augustinack JC, Wiggins G, Wald LL, Diana Rosas H, Pothast A, Schwartz EL, Fischl B. 2008. Accurate prediction of V1 location from cortical folds in a surface coordinate system. *Neuroimage*. 39:1585–1599.
- Kaas JH. 2000. Why is brain size so important: design problems and solutions as neocortex gets bigger or smaller. *Brain Mind*. 1:7–23.
- Kanai R, Bahrami B, Rees G. 2010. Human parietal cortex structure predicts individual differences in perceptual rivalry. *Curr Biol*. 20:1626–1630.
- Kanai R, Carmel D, Bahrami B, Rees G. 2011. Structural and functional fractionation of right superior parietal cortex in bistable perception. *Curr Biol*. 21:R106–R107.
- Kanai R, Rees G. 2011. The structural basis of inter-individual differences in human behaviour and cognition. *Nat Rev Neurosci*. 12:231–242.
- Kang MS, Blake R. 2011. An integrated framework of spatiotemporal dynamics of binocular rivalry. *Front Hum Neurosci*. 5:88.
- Kang MS, Heeger D, Blake R. 2009. Periodic perturbations producing phase-locked fluctuations in visual perception. *J Vis*. 9:8.
- Kang MS, Lee SH, Kim J, Heeger D, Blake R. 2010. Modulation of spatiotemporal dynamics of binocular rivalry by collinear facilitation and pattern-dependent adaptation. *J Vis*. 10:3.
- Knapen T, van Ee R, Blake R. 2007. Stimulus motion propels traveling waves in binocular rivalry. *PLoS One*. 2:e739.
- Kornack DR, Rakic P. 1995. Radial and horizontal deployment of clonally related cells in the primate neocortex: relationship to distinct mitotic lineages. *Neuron*. 15:311–321.
- Lee SH, Blake R. 2002. V1 activity is reduced during binocular rivalry. *J Vis*. 2(9):4.
- Lee SH, Blake R, Heeger DJ. 2007. Hierarchy of cortical responses underlying binocular rivalry. *Nat Neurosci*. 10:1048–1054.
- Lee SH, Blake R, Heeger DJ. 2005. Traveling waves of activity in primary visual cortex during binocular rivalry. *Nat Neurosci*. 8:22–23.
- Leuba G, Garey LJ. 1987. Evolution of neuronal numerical density in the developing and aging human visual cortex. *Hum Neurobiol*. 6:11–18.
- Meenes M. 1930. A phenomenological description of retinal rivalry. *Am J Psychol*. 42:260–269.
- Moradi F, Heeger DJ. 2009. Inter-ocular contrast normalization in human visual cortex. *J Vis*. 9:13.
- Muckli L, Kohler A, Kriegeskorte N, Singer W. 2005. Primary visual cortex activity along the apparent-motion trace reflects illusory perception. *PLoS Biol*. 3:e265.
- Muthukumaraswamy SD, Edden RAE, Jones DK, Swettenham JB, Singh KD. 2009. Resting GABA concentration predicts peak gamma frequency and fMRI amplitude in response to visual stimulation in humans. *Proc Natl Acad Sci USA*. 106:8356–8361.
- Naber M, Carter O, Verstraten FAJ. 2009. Suppression wave dynamics: visual field anisotropies and inducer strength. *Vision Res*. 49:1805–1813.
- Oldfield RC. 1971. The assessment and analysis of handedness: the Edinburgh inventory. *Neuropsychologia*. 9:97–113.
- Paffen CLE, Naber M, Verstraten FAJ. 2008. The spatial origin of a perceptual transition in binocular rivalry. *PLoS One*. 3:e2311.
- Panizzon MS, Fennema-Notestine C, Eyerly LT, Jernigan TL, Prom-Wormley E, Neale M, Jacobson K, Lyons MJ, Grant MD, Franz CE et al. 2009. Distinct genetic influences on cortical surface area and cortical thickness. *Cereb Cortex*. 19:2728–2735.
- Pearson J, Tadin D, Blake R. 2007. The effects of transcranial magnetic stimulation on visual rivalry. *J Vis*. 7:2.1–2.11.
- Pelli DG. 1997. The VideoToolbox software for visual psychophysics: transforming numbers into movies. *Spat Vis*. 10:437–442.
- Peña EA, Slate EH. 2006. Global validation of linear model assumptions. *J Am Stat Assoc*. 101:341.
- Pitzalis S, Galletti C, Huang RS, Patria F, Committeri G, Galati G, Fattori P, Sereno MI. 2006. Wide-field retinotopy defines human cortical visual area V6. *J Neurosci*. 26:7962–7973.
- Polonsky A, Blake R, Braun J, Heeger DJ. 2000. Neuronal activity in human primary visual cortex correlates with perception during binocular rivalry. *Nat Neurosci*. 3:1153–1159.
- Pöppel E, Brinkmann R, von Cramon D, Singer W. 1978. Association and dissociation of visual functions in a case of bilateral occipital lobe infarction. *Arch Psychiatr Nervenkr*. 225:1–21.
- Rakic P. 1995. A small step for the cell, a giant leap for mankind: a hypothesis of neocortical expansion during evolution. *Trends Neurosci*. 18:383–388.
- Schira MM, Tyler CW, Breakspear M, Spehar B. 2009. The foveal confluence in human visual cortex. *J Neurosci*. 29:9050–9058.
- Schwarzkopf DS, Rees G. 2013. Subjective size perception depends on central visual cortical magnification in human V1. *PLoS One*. 8(3): e60550.
- Schwarzkopf DS, Robertson DJ, Song C, Barnes GR, Rees G. 2012. The frequency of visually induced gamma-band oscillations depends on the size of early human visual cortex. *J Neurosci*. 32:1507–1512.
- Schwarzkopf DS, Song C, Rees G. 2011. The surface area of human V1 predicts the subjective experience of object size. *Nat Neurosci*. 14:28–30.
- Sereno MI, Dale AM, Reppas JB, Kwong KK, Belliveau JW, Brady TJ, Rosen BR, Tootell RBH. 1995. Borders of multiple visual areas in humans revealed by functional magnetic resonance imaging. *Science*. 268:889–893.

- Uhlhaas PJ, Pipa G, Lima B, Melloni L, Neuenschwander S, Nikolić D, Singer W. 2009. Neural synchrony in cortical networks: history, concept and current status. *Front Integr Neurosci.* 3:17.
- van Pelt S, Boomsma DI, Fries P. 2012. Magnetoencephalography in twins reveals a strong genetic determination of the peak frequency of visually induced gamma-band synchronization. *J Neurosci.* 32:3388–3392.
- Wandell BA, Dumoulin SO, Brewer AA. 2007. Visual field maps in human cortex. *Neuron.* 56:366–383.
- Wheatstone C. 1838. Contributions to the physiology of vision. Part the first. On some remarkable, and hitherto unobserved, phenomena of binocular vision. *Phil Trans R Soc Lond.* 128:371–394.
- Wilson HR, Blake R, Lee SH. 2001. Dynamics of travelling waves in visual perception. *Nature.* 412:907–910.
- Winkler AM, Kochunov P, Blangero J, Almasy L, Zilles K, Fox PT, Dugirala R, Glahn DC. 2010. Cortical thickness or grey matter volume? The importance of selecting the phenotype for imaging genetics studies. *Neuroimage.* 53:1135–1146.
- Wolfe JM. 1984. Reversing ocular dominance and suppression in a single flash. *Vision Res.* 24:471–478.
- Wunderlich K, Schneider KA, Kastner S. 2005. Neural correlates of binocular rivalry in the human lateral geniculate nucleus. *Nat Neurosci.* 8:1595–1602.
- Zaretskaya N, Thielscher A, Logothetis NK, Bartels A. 2010. Disrupting parietal function prolongs dominance durations in binocular rivalry. *Curr Biol.* 20:2106–2111.
- Zhang P, Jamison K, Engel S, He B, He S. 2011. Binocular rivalry requires visual attention. *Neuron.* 71:362–369.